RSC Advances

PAPER

View Article Online
View Journal | View Issue

Cite this: *RSC Adv.*, 2026, **16**, 17574

A fluorometric chemosensor for the sequential determination of Fe(III) and cefotaxime sodium in water samples, serum and commercial formulations: a computational and an experimental approach

Ikram Ullah, *[a] Mian Muhammad, *[a] Faiz Ali, *[a] Zakir Zaman Khan,[b] Sikander Khan[a] and Fatima Bibi[a]

An indole-based chemosensor (P1) was synthesized and characterized using FT-IR and ^{1}H NMR and was investigated fluorometrically for the determination of various metal ions. It was found that Fe(III) caused significant quenching compared to other metal ions, resulting in the formation of a non-fluorescent complex P1/Fe(III). Subsequently, the complex P1/Fe(III) represented as P2 was further utilized as a chemosensor for detecting cefotaxime sodium (CFT), an antibiotic. The fluorescence intensity of P2 was significantly decreased by the introduction of CFT into the complex mixture. Under optimum conditions, the linearity was found in the range of 0.3–3.0 μg mL^{-1} for Fe(III) and 0.5–5 μg mL^{-1} for CFT, and the LOD and LOQ were calculated to be 0.08 μg mL^{-1} and 0.28 μg mL^{-1} for Fe(III), and 0.12 μg mL^{-1} and 0.4 μg mL^{-1} for CFT, respectively. In addition, a theoretical study using DFT and QTAIM analyses predicted the formation of a thermodynamically feasible complex between the P1 and Fe(III) and CFT, stabilized by van der Waals forces and a dative-type of interaction. Furthermore, the probe P1 was applied for the determination of Fe(III) in water samples, and P2 was employed for the determination of CFT in serum samples and commercial formulations.

Received 9th December 2025
Accepted 24th March 2026

DOI: 10.1039/d5ra09532h

rsc.li/rsc-advances

1. Introduction

In recent years, environmental contamination with heavy metal ions has become a serious concern.[1,2] The development of methods to detect environmentally and biologically important species has received great interest in the research field of chemical sensors.[3] Among different heavy metal ions, Fe(III) is the most vital and abundant transition metal in plants and the human body. It performs a significant role in enzymatic catalysis and cellular metabolism. It serves as a carrier for oxygen and electron transport in hemoglobin and as a cofactor in certain enzymatic reactions.[4] Iron(III) is essential for the living body, but at higher concentrations it can cause damage to nucleic acids, cellular lipids and proteins respectively. On the other hand, deficiency of Fe(III) limits the oxygen supply to cells and causes anemia, kidney and liver damage, diabetes and heart problems.[5–9] According to the WHO, the maximum permissible level of iron in drinking water is 0.3 mg L^{-1}. However, release of industrial and domestic waste into water is responsible for the increased iron levels.[10]

Antibiotics have fundamental applications in improving human health against infectious diseases as well as being used in treating and preventing plant and animal infections.[11] The consumption of antibiotics globally in animals is almost double that of consumed by humans.[12]

Among antibiotics, cephalosporins are a bactericidal class of antibiotics. Cefotaxime sodium (CFT) is marketed by the common trade name Claporan and its IUPAC name is "Sodium-3-[(acetyloxy)methyl]-7-[[(2*Z*)-2-(2 aminothiazol-4-yl)-2-(methoxyimino) acetyl] amino]-8-oxo-5-thia-1-azabicyclo [4.2.0] oct 2-ene-2-carboxylate" (Fig. 1a).[13] Cefotaxime sodium is a broad-spectrum beta-lactam antibiotic and is used for the treatment of skin, stomach, respiratory tract, ears, sinuses, blood, brain, and urinary tract infections.[14] Humans release antibiotic contents into the ecosystem primarily through the excretion of urine, feces, and hospital effluents as well as during the production of antibiotics.[15] The major disadvantage of antibiotic discharge into the natural environment is the selection of resistant bacteria.[16] Other side effects associated with antibiotics include disrupting microbial processes such as organic matter degradation and nitrogen transformation in water, soil, livestock manure treated with antibiotics, affecting crops and entering into the food. Non-

[a]*Department of Chemistry, University of Malakand, Khyber Pakhtunkhwa, Pakistan. E-mail: ikramullah629@gmail.com; mianchem@uom.edu.pk; faizy186@gmail.com; faiz@uom.edu.pk*

[b]*Government Degree College Gulabad, Higher Education Archives and Libraries Department, Dir Lower, 18800, Khyber Pakhtunkhwa, Pakistan*

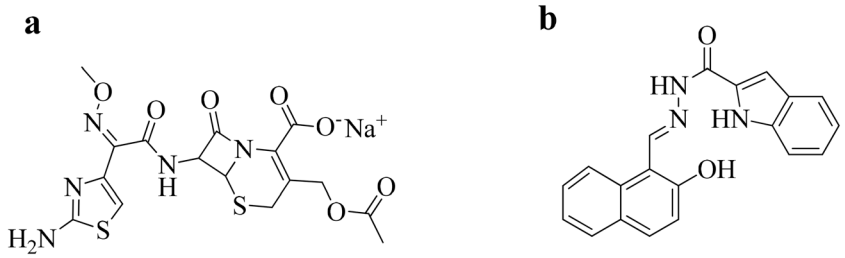

Fig. 1 Chemical structures of (a) cefotaxime sodium (CFT) and (b) chemosensor P1.

target organisms like micro-invertebrates, *i.e.*, Daphnia magna and Artemia, fish and amphibians can also be affected due to the excessive amount of antibiotics.[17]

The development of analytical methods for the detection, and monitoring of antibiotic levels in various matrices such as serum, commercial formulations and water, is necessary to explore and protect the public health and environment from the adverse consequences of antibiotic pollution.

Different methods have been applied for the detection of Fe(III), including inductively coupled plasma mass spectrometry (ICP-MS),[18] flame atomic absorption spectrometry (FAAS),[19] high performance liquid chromatography (HPLC),[20] colorimetric,[21] electrochemical,[22] electron probe microanalysis (EPMA)[23] and spectrophotometric methods[24] *etc.* Similarly, the techniques used for the determination of cefotaxime sodium antibiotic are spectrophotometric,[25] electrochemical,[26] and reversed-phase high-performance liquid chromatography (RP-HPLC).[27] Accurate determination can be obtained by these methods with sufficient selectivity and sensitivity, but usually they need expensive instrumentation, high reagent loss, pre-treatment time, are difficult to operate, and need long analysis time. In contrast, a spectrofluorimetric method is preferred based on easy operation, fast analysis and cost-effectiveness with good response towards the target analytes.[28]

Schiff's bases are widely used on biological sites, such as antibacterial, antifungal, anti-inflammatory and antioxidants as well as metal complexes formation and dyes and pigments industries.[29] Similarly, they are well-known organic compounds for their significant contribution in the research field of sensing due to the presence of electron rich centers as receptors *i.e.* N atom in the azomethine group, for effective coordination.[30] Hence, chemosensors with selective, multifunctional, low-cost and sensitive detection of analytes have been emerging and challenging approach. Among these organic chemosensors, indole-based Schiff's base derivatives have been extensively designed as chemosensors for determining various ions because of their unique photophysical properties, good water solubility, biocompatibility and essential role in biological systems.[31]

This study focuses on developing a reliable and efficient chemosensor, "(*E*)-*N*′-((2-hydroxynaphthalen-1-yl) methylene)-1*H*-indole-2-carbohydrazide", represented as P1 (Fig. 1), based on fluorescence quenching for the determination of Fe(III), and subsequently, the resulting complex (P2) was investigated for the determination of CFT. Various parameters for optimization, including the effect of concentration of P1, pH, solvents, and kinetic stability, were studied to assist in achieving the maximum signal for the determination of Fe(III) and cefotaxime sodium. Statistical parameters such as standard deviation, limit of detection, limit of quantification, and percent relative standard deviation were also calculated to determine the robustness, precision, and accuracy of the proposed method. The proposed method was applied for the determination of Fe(III) in water samples as well as P2 was used for the determination of Cefotaxime sodium in serum and commercial formulation. In addition, the results of the proposed method were compared to the reported techniques, showing superior performance in real sample analysis.

2. Experimental

2.1. Chemicals

All chemicals used in this study were of analytical grade and were not further purified. Metal salts of $SnCl_2$, $AlCl_3$, $PbCl_2$, $HgCl_2$, $FeCl_3$, $CrCl_3$, $CuCl_2$, $AgNO_3$, *etc.* were received from Sigma Aldrich. The starting materials for the synthesis of the target compound were ethyl 1*H*-indole-2-carboxylate, 2-hydroxy-1-naphthaldehyde and hydrazine. Acids such as boric acid (ACS reagent grade), acetic acid (ACS reagent, 99.7%), and phosphoric acid (85%) were used to prepare the Britton Robinson Buffer, and sodium hydroxide (Sigma-Aldrich, Germany) was used to adjust the pH to the required level. A sample of cefotaxime sodium antibiotic was supplied from "Sami Pharmaceuticals (PVT) LTD Pakistan". Commercially formulated injection of the cefotaxime sodium formula was purchased from the local market, and a serum sample was provided by Master Lab, located near the Tehsil Headquarters Hospital Chakdara, Dir Lower, Pakistan, for the determination of cefotaxime sodium in the given samples.

2.2. Instrumentation

For measuring fluorescence, a spectrofluorophotometer (RF-5301 PC, Shimadzu, Japan) with a 150-watt xenon lamp and a quartz cell (l.0 cm) was used. Measurement of pH was done using an analog pH meter (Model PHS-3BW, 2908 N, Chicago, USA). A hot plate/magnetic stirrer (Irmico, Germany) was used for heating and stirring purposes. To monitor the reaction progress, thin layer chromatographic plates (TLC) were used, and spots were observed under a UV lamp. Infrared spectra (cm^{-1}) were recorded on Bio-Rad FTS 3000 MX in the range of 500–4000 cm^{-1} with a KBr disc. NMR characterization was done on a BRUKER AVANCE NEO spectrophotometer at 500 MHz.

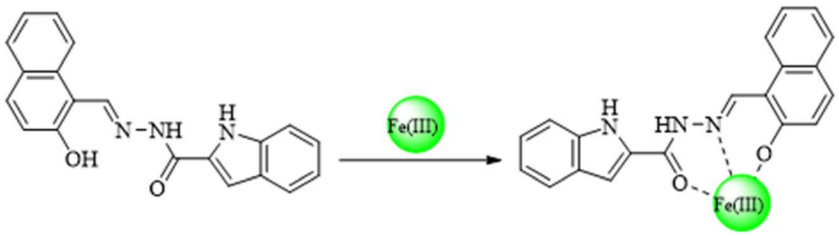

Scheme 1 Proposed sensing mechanism of P1 with Fe(III).

The chemical shifts (δ) are measured in parts per million (ppm) downfield from the internal standard tetramethyl silane (TMS). Chloroform was used as a solvent. The SMPI Melting point apparatus was used for the determination of melting points (m.p.) and are uncorrected.

2.3. Solutions

Stock solutions (100 μg mL^{-1}) of chemosensor P1 in methanol, $FeCl_3$ and cefotaxime sodium in distilled water were prepared. Britton Robinson Buffer was prepared by mixing acid solutions of CH_3COOH, H_3PO_4 and H_3BO_3, each at a concentration of 0.04 M. Buffer solutions having variable pH were prepared by adding NaOH (0.2 M) solution to the appropriate volume of the acid mixture.

2.4. Synthesis of chemosensor

The indole hydrazone derivative compounds, previously assayed for antioxidant, photoprotective and antiproliferative activity and recently used as a chemosensor (P1), was synthesized according to the reported literature.[32] Ethyl 1*H*-indole-2-carboxylate (0.5 g, 2.6 mmol) was dissolved in methanol (20 mL), added a few drops of acetic acid serving as a catalyst and stirring the solution vigorously for 15 min. Subsequently, hydrazine hydrate (0.4 mL, 2.6 mmol) was added to the mixture, and the reaction mixture was refluxed until the compound formation was confirmed through a TLC study observed under UV. In the next step, 2-hydroxy-1-naphthaldehyde (0.45 g, 2.6 mmol) in 15 mL of methanol was subjected to the product formed in the first step, stirred and refluxed the mixture at 70 °C till the confirmation of the product P1 was observed through a TLC study, as shown (SI File 1-Scheme 1). Yield 69%. Chemical formula: $C_{20}H_{15}N_3O_2$, molecular weight: 328.932, m.p. = 252–256 °C (CH_3OH). IR (KBr, cm^{-1}) ν 3100–3304 broad peak (N–H, and O–H), 1686 (CO), 1618 (C=N–), 1527 (C=C), 1308 (C–O), 1248 (C–N).^{1}H NMR (δ in ppm, 500 MHz, J in Hz, solvent $CDCl_3$): 12.3 (s, NH), 9.67 (s, NH), 8.79 (s, CH), 5.53 (s, –OH), 7.99 (d, 1H), 7.89 (d, 1H), 7.78 (d,1H), 7.70 (d, 1H), 7.43 (m, 3H), 7.34 (d, 1H), 7.19 (d, 1H), 7.14 (t, 2H).

2.5. General procedure

All the working solutions were made in a series of 5.0 mL volumetric flasks. A 15 μg mL^{-1} solution of chemosensor P1 was prepared from a 100 μg mL^{-1} stock solution of P1 and a variable volume of Fe(III) solution (10 μg mL^{-1}) corresponding to concentrations in the range of 0.3, 0.5, 0.8, 1.0, 1.4, 1.8, 2.2, 2.6, and 3.0 μg mL^{-1} was added. In all the solution mixtures, P1 concentration was maintained at 15 μg mL^{-1}. After dilution, when required, fluorescence measurements were conducted at λ_{em} = 420 nm following excitation at λ_{ex} = 320 nm against reagent blanks. Subsequently, different volumes of cefotaxime sodium solution (50 μg mL^{-1}) corresponding to concentrations of 0.5, 1.0, 2.0, 3.0, 4.0, and 5.0 μg mL^{-1} upon dilution up to the mark were added to the mixture of P1 (15 μg mL^{-1}) and Fe(III) (2.0 μg mL^{-1}), and the fluorescence at λ_{em} = 420 nm was measured. The blank solution of P1 (15 μg mL^{-1}) was prepared without the addition of Fe(III), and a blank solution of P2 was made without the addition of cefotaxime sodium. All readings were taken in neutral medium. $F^\circ - F$ and sequentially $F^\circ - F'$ was calculated in each case against the increasing concentration of Fe(III) and Cefotaxime sodium respectively. Here, F° shows the fluorescence intensity (FI) of P1, whereas F is the FI of P2 and F' is the FI of P2-CFT.

2.6. Optimization studies

2.6.1. Effect of pH. To demonstrate the effect of pH on the fluorescence quenching of P1, a series of solutions was prepared having P1 (15 μg mL^{-1}) and Fe(III) (1.0 μg mL^{-1}) in volumetric flasks of 5.0 mL. Then, added 2.0 mL of buffer of pH ranging from 2 to 12 in series to each flask and diluted with distilled water up to the mark. The blank was also prepared without the addition of Fe(III) and the emission intensity was measured against the blank solution in each case at 420 nm. Furthermore, the P1/Fe(III) complex now represented as P2 was used as a chemosensor at an optimum pH for the determination of cefotaxime sodium antibiotic.

2.6.2. Effect of concentration of P1 on its interaction with Fe(III). To explore the concentration of P1 that leads to maximum quenching upon the addition of Fe(III), solutions with different concentrations of P1 (5.0, 10, 15 and 20 μg mL^{-1}) were prepared by adding calculated volume from 100 μg mL^{-1} solution of P1 with a constant concentration of Fe(III) (1.0 μg mL^{-1}) and dilution was done with distilled water and methanol up to the mark in 5.0 mL volumetric flasks, serially. Fluorescence was recorded for each solution at 420 nm against the respective blank.

2.6.3. Effect of solvents. The effect of different solvents such as dimethyl sulfoxide (DMSO), acetonitrile (ACN), dimethyl formamide (DMF), methanol, and water on changes in the fluorescent intensity (FI) was studied to achieve maximum signal response of P1 and its quenching on interaction with Fe(III). The concentrations of P1 and Fe(III) were maintained at

15 μg mL^{-1} (0.75 mL from 100 μg mL^{-1}) and 1.0 μg mL^{-1} (0.5 mL from 10 μg mL^{-1}) in a series of 5.0 mL volumetric flasks and diluted with relevant solvents separately. The blank solution of P1 in different solvents was also made as a reference without the analyte Fe(III). Fluorescence intensity was measured and plotted $F^{\circ} - F$ against respective solvents.

2.6.4. Kinetic stability and reaction time. The interaction of P1 and Fe(III) as well as stability, was explored as a function of time for an hour. The solution of P1 (15 μg mL^{-1}) and Fe(III) (1.0 μgmL^{-1}) was prepared in a 5 mL volumetric flask. Fluorescence intensity at 420 nm against the respective blank was monitored with an interval of 10 min and the figure was constructed as a function of time.

2.7. Interference effect

The effect of metal ions and common excipients on the determination of Fe(III) and cefotaxime sodium was explored. Mixtures of P1 (15 μg mL^{-1}) and different metal ions (1.0 μg mL^{-1}) were prepared individually in 5.0 mL volumetric flasks. On the other hand, for co-existing interference study, different metal ions solutions such as Co(II), Pb(II), Na(I), Fe(II), Pd(II), Sn(II), Cd(II), Mg(II), Ni(II), Ca(II), Ag(I), Mn(II), K(I), Zn(II), and Hg(II) were prepared each having concentration of 2.0 μg mL^{-1} and mixed with 0.75 mL of P1 (100 μg mL^{-1}) and 0.5 mL of Fe(III) (10 μg mL^{-1}) in a series of 5.0 mL volumetric flasks individually and dilution was done up to the mark with distilled water. The blank (a mixture of P1 and Fe(III)) was made excluding other metal ions. The selectivity of P2 was further explored towards CFT. The effect of common excipients, *i.e.*, fructose (Fru), glucose (Glu), citric acid (C acid), folic acid (F acid), galactose (Gal), gum and antibiotics including cefepime (Cef), linezolid (LIN), and ceferazone sodium (CNa) on the determination of CFT was investigated. A 0.75 mL of P1 (100 μg mL^{-1}), 0.5 mL of Fe(III) (10 μg mL^{-1}) and 0.5 mL of CFT (10 μg mL^{-1}) were mixed with 1.0 mL of each excipient from 100 μg mL^{-1} stock solution in 5.0 mL volumetric flasks, serially diluted with distilled water up to the mark. Similarly, the same method was proceeded to find out the interference effect of different metal ions on the determination of CFT using P2 as for common excipients. The fluorescence intensity was measured against the respective blank.

2.8. Computational study

Density functional theory (DFT) calculations were carried out *via* the DMol^3 module to substantiate the interaction of P1 with Fe(III) and CFT.[33] The Perdew–Burke–Ernzerhof (PBE) functional of the Generalized-Gradient-Approximation (GGA) was employed to account for the electron exchange–correlation terms in all the energy calculations.[34] Similarly, the double-numerical-plus-polarization (DNP) was selected as the atomic-orbital basis set and the DFT semi-core pseudopotential (DSSSP) was taken to consider the relativistic effect. Whereas the smearing and global orbital cutoff radius were chosen as 0.005 Ha and 4.6 Å, respectively. Moreover, the Grimme scheme of the DFT-D3 was adopted to deal with the van der Waals forces and other long–range interactions.[35] In addition, the convergence criterion for structure relaxation were set as 10^{-5} Ha, 0.002 Ha $Å^{-1}$, and 0.005 Å for energy, maximum force, and displacement, respectively. Similarly, the effect of water as a solvent was incorporated through the conductor-like screening model (COSMO) with a dielectric constant value of 78.5, during all calculations.[36] Furthermore, the binding energy (E_b) was calculated as:

$$E_b = E_{P1/Fe(III)} - (E_{P1} + E_{Fe(III)}) \quad \text{(i)}$$

$$E_b = E_{P2\text{-}CFT} - (E_{P2} + E_{CFT}) \quad \text{(ii)}$$

$$E_b = E_{P\text{-}CFTCl} - (E_{P2\text{-}CFT} + E_{Cl})$$

where E_{P1}, E_{CFT}, $E_{Fe(III)}$, E_{Cl}, E_{P2}, $E_{P2\text{-}CFT}$, and $E_{P2\text{-}CFTCl}$ illustrate the optimized energies of P1, CFT, Fe(III), Cl, Fe-bonded P1, P2-CFT, and the overall complex, respectively.

The Quantum theory of atoms in molecules (QTAIM) and the non-covalent interaction (NCI) reduced density gradient (NCI-RDG) analyses were performed using the Multiwfn 3.7 and visual molecular dynamics (VMD) program, whereas the input files were generated by Gaussian 16 package.[37–40] The QTAIM topological parameters, such as all electron density "$\rho(r)$", laplacian of the electron density "$\nabla^2\ \rho(r)$", and total electron energy density "$H(r)$ at the bond critical points (BCPs) between nuclei were computed to characterize the nature and strength of interactions.

2.9. Applications

The practical application of the proposed method was checked as a spiking study. For this purpose, tap water and river water were received from the local area near the University Campus. The suspended particles of pond water were removed through filtration. Next, 0.5 mL of P1 (100 μg mL^{-1}) and the calculated volume of Fe(III) (0.5, 1.0 mL) from 10 μg mL^{-1} were added into 5.0 mL volumetric flasks serially and diluted up to the mark with pond water. The same process was repeated using tap water. Similarly, blank solutions of P1 were prepared in tap and pond water, excluding Fe(III) addition as a reference, and FI was measured at $\lambda_{em} = 420$ nm.

Furthermore, P2 was explored as a sensing probe for the determination of CFT antibiotic in serum and commercial formulation samples. To separate plasma from blood, centrifugation was done for 5 minutes, and plasma was collected through a syringe. After that, 4.0 mL of plasma was spiked with 2.0 mL of standard CFT (100 μg mL^{-1}), then acetonitrile (ACN) (4.0 mL) was added as a deproteinating agent of plasma proteins. This mixture has a total volume of 10 mL with CFT concentration of 20 μg mL^{-1}. Again, centrifugation was performed for 10 min., and the supernatant serum (5.0 mL) was transferred to a 10 mL volumetric flask and diluted to the mark with distilled water, resulting in a 10 μg mL^{-1} concentration of CFT. Taken 0.75 mL of P1 (100 μg mL^{-1}) and 0.5 mL of Fe(III) (10 μg mL^{-1}) mixed with 0.5 mL and 1.0 mL serially in 5.0 mL flasks, which give 1.0 and 2.0 μg mL^{-1} concentration of CFT, respectively. The blank was made as such, excluding the CFT. In

addition, injection of cefotaxime sodium (cefotax 0.250 gm) was bought from the local market. An amount of 0.005 g was dissolved in 100 mL of distilled water, making a 50 μg mL^{-1} stock solution. Working solutions were made in 5.0 mL volumetric flasks by mixing 0.75 mL of P1 (100 μg mL^{-1}), 0.5 mL of Fe(III) (10 μg mL^{-1}) and 0.1 mL and 0.2 mL of CFT (50 μg mL^{-1}), which formed 1.0 μg mL^{-1} and 2.0 μg mL^{-1} concentrations of CFT, respectively and diluted up to the mark with distilled water. The blank solution was made in a similar way, excluding the cefotaxime sodium (Inj. Cefotax) and fluorescence was recorded at λ_{em} = 420 nm against the respective blank.

3. Results and discussion

3.1. Characterization

The chemosensor P1 was synthesized and characterized using various techniques, including FTIR and ^{1}H NMR (SI File 2 and 3). The FTIR spectra of the compound gives a broad stretch peak in the range of 3100 to 3304 cm^{-1} representing the –NH groups and –OH group. The peak at 1688 shows C=O (carbonyl group), and the appearance of a new peak at 1618 cm^{-1} represents –C=N–, indicating the formation of Schiff's base. Furthermore, the peaks at 1527, 1308 and 1248 cm^{-1} show C=C, C–O (phenolic), and C–N, respectively. On the other hand, the broad stretch peak in the range of 3100 to 3300 cm^{-1} of P1 for OH and NH become short when Fe(III) was added. The imine group that appeared at 1618 cm^{-1} is also shifted to lower frequency range 1604 cm^{-1} indicating the coordination of –OH and –C=N– with Fe(III) as suggested in proposed sensing mechanism between P1 and Fe(III). Thus, the characteristic bands of the relevant groups confirm the structure of the compound P1 and the proposed sensing scheme of P1 with Fe(III), as shown in SI 1a and b. As shown in SI 2, the peaks found at 12.3 (singlet), 9.67 (singlet), 8.79 (singlet), 5.53 (singlet) ppm show the protons of –NH indole ring, –HN–N, HC=N–, and –OH and the remaining peaks at 7.99 (doublet), 7.89 (doublet), 7.78 (doublet), 7.70 (doublet), 7.43 (multiplet), 7.34 (doublet), 7.19 (doublet), 7.14 (triplet), showing the aromatic and indole ring protons respectively.

3.2. Fluorescence study

The fluorescent behavior of the chemosensor P1 (emission at 420 nm followed excitation at 320 nm) upon interaction with different metal ions such as Mn(II), Na(I), Ca(II), Cr(III), Ag(I), Cu(II), Zn(II), Al(III), Zn(II), Fe(III), Mg(II), Fe(II), Cd(II), Ni(II), and Co(II) was explored. It was observed that Fe(III) causes a significant decrease in the fluorescent intensity (FI) of P1 as compared to other metal ions (Fig. 2a), indicating a strong selective interaction between P1 and Fe(III), leading to the formation of a P2 as shown schematically in Scheme 1. Other metal ions interacted at quite low levels, which can be considered negligible. Consequently, quantitative determination of Fe(III) was carried out using P1 as a chemosensor, which proved to be a reliable approach.

Furthermore, cefotaxime sodium (CFT) antibiotic was detected using P2 complex as a sensing probe. The method was based on further quenching in FI caused by antibiotic CFT upon interaction with P2 complex, leading to the formation of non-fluorescent products. The selectivity of the P2 complex for the detection of CFT antibiotic was investigated in the presence of certain antibiotics and common excipients, exhibiting no interference effect. Thus, P1 was used as a selective dual chemosensing probe for the determination of Fe(III) and subsequently P2 for the determination of CFT. The result is shown in Fig. 2b.

3.3. Effect of pH

The pH of the medium has a profound effect on the determination of analytes having either acidic or basic nature, and the

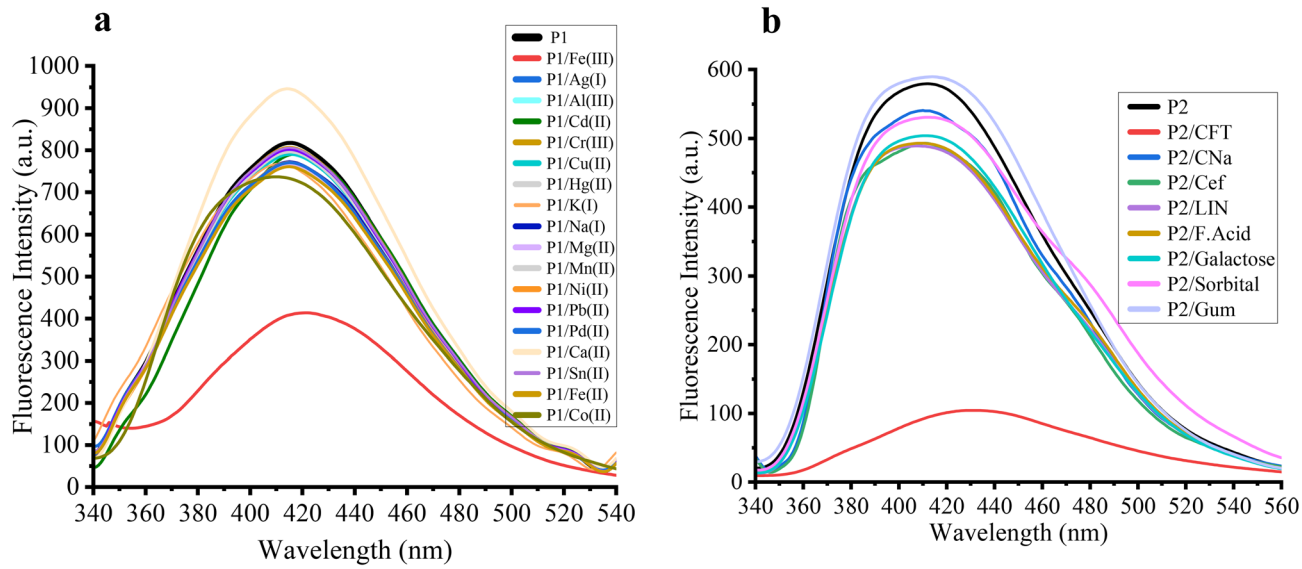

Fig. 2 (a) Interactions of different metal ions with chemosensor P1 (b) fluorescence quenching of P2 upon interaction with CFT, antibiotics and other common excipients.

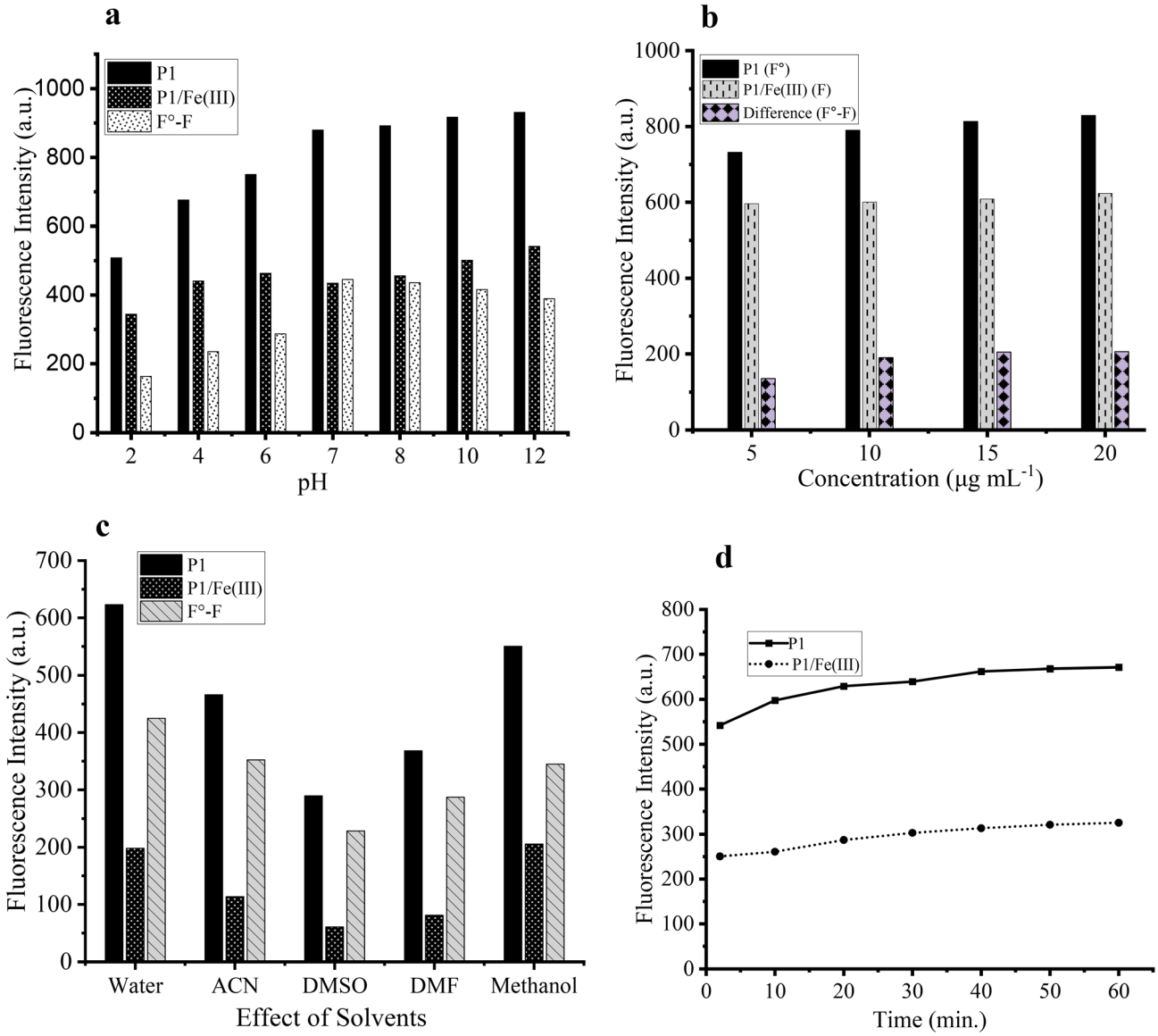

Fig. 3 (a). The effect of pH on the sensing response of P1 to Fe(III). (b) The effect of the concentration of P1 on fluorescence quenching caused by Fe^{3+}. (c) The effect of different solvents on the fluorescence intensity of P1 and P1/Fe(III). (d) Stability and reaction time of P1 with Fe(III).

chemosensors used for sensing.[41] The influence of pH was investigated in the range of 2–12 and the results are shown in Fig. 3a. It was observed that under the acidic pH (2–6) the P1 fluorescent quenching was not significant. A possible reason could be the protonation of the imine group in P1, which prevents the interaction of Fe(III).[42] At pH above 8, the Fe(III) ions are surrounded by OH^- ions, reducing their interaction with P1. Therefore, pH 7 was selected as the optimum pH for Fe(III) detection. At this optimum pH, CFT determination was also explored.

3.4. Effect of P1 concentration

To estimate the optimum concentration of P1 at which Fe(III) caused maximum fluorescence quenching, a constant concentration of Fe(III) (1.0 μg mL^{-1}) was reacted with different concentrations of P1 in the range of 5–20 μg mL^{-1}, and FI was measured. As shown in Fig. 3b, the interaction of Fe(III) was maximum at 15 μg mL^{-1} of P1 and remains unchanged beyond the optimum concentration. This indicated that the binding of all the Fe(III) ions to P1 and fluorescence quenching remains constant beyond optimum concentration.

3.5. Effect of solvents on the fluorescence of P1 and its interaction with Fe(III)

The fluorescence of P1 and its complex with Fe(III) in different solvents, including DMSO, DMF, methanol, ACN, and water, was investigated. It was observed, as shown in Fig. 3c, that the fluorescence intensity of P1 is maximum in water, as well as Fe(III), which causes maximum quenching as compared to other solvents. The most possible explanation is that Schiff's bases are freely soluble in organic solvents, resulting in the loss of energy non-radiatively due to the free rotation of the

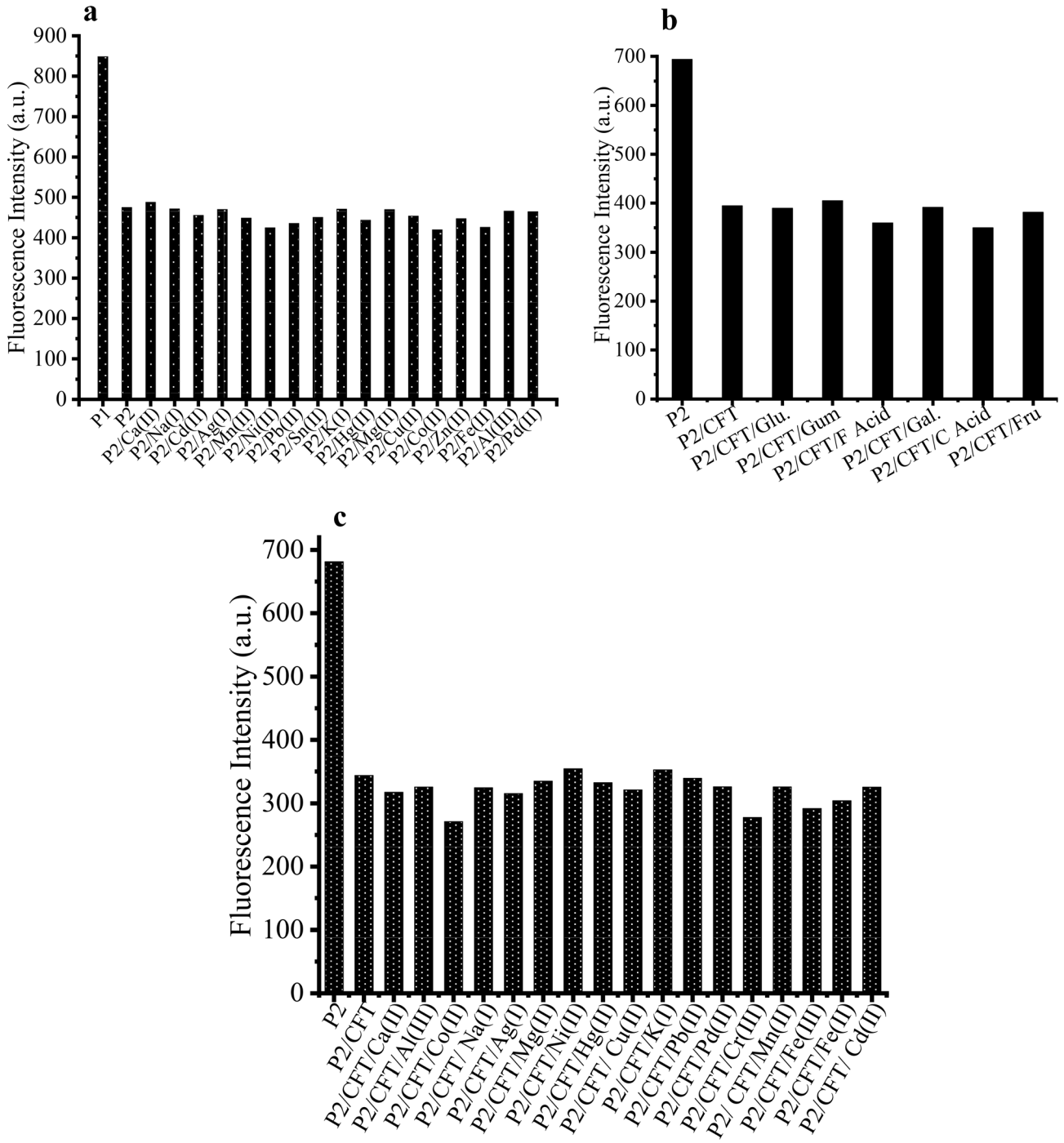

Fig. 4 (a) Co-existing metal ions effect on the fluorescence intensity of P2. (b) Effect of common excipients on the determination of CFT using P2 (c) interference effect of different metal ions on the determination of CFT.

singly bonded groups *i.e.* C–N bond of hydroxy aromatic aldehyde rings. On the other hand, as the fraction of water increases in methanol, the fluorescence intensity of P1 enhances due to the poor solubility; as a result, free rotation is inhibited, which attenuates the decay of non-radiation called "Aggregation Induced Enhanced Emission" (AIEE). In contrast, the combination of P1 and Fe(III) inhibited the "Excited state intramolecular proton transfer" (ESIPT) as well as intramolecular charge transfer (ICT) activated towards metal ions, leading to the maximum fluorescence of P1 being quenched by Fe(III).[43]

3.6. Stability as a function of time

The stability of P1 and its complex with Fe(III) with respect to time was investigated. As shown in Fig. 3d, the P1 and P2 (P1/Fe(III)) exhibited comparatively high stability in the solvent system of methanol to water (2 : 3 v/v). In Schiff's bases, when the imine group is conjugated with aromatic rings or other

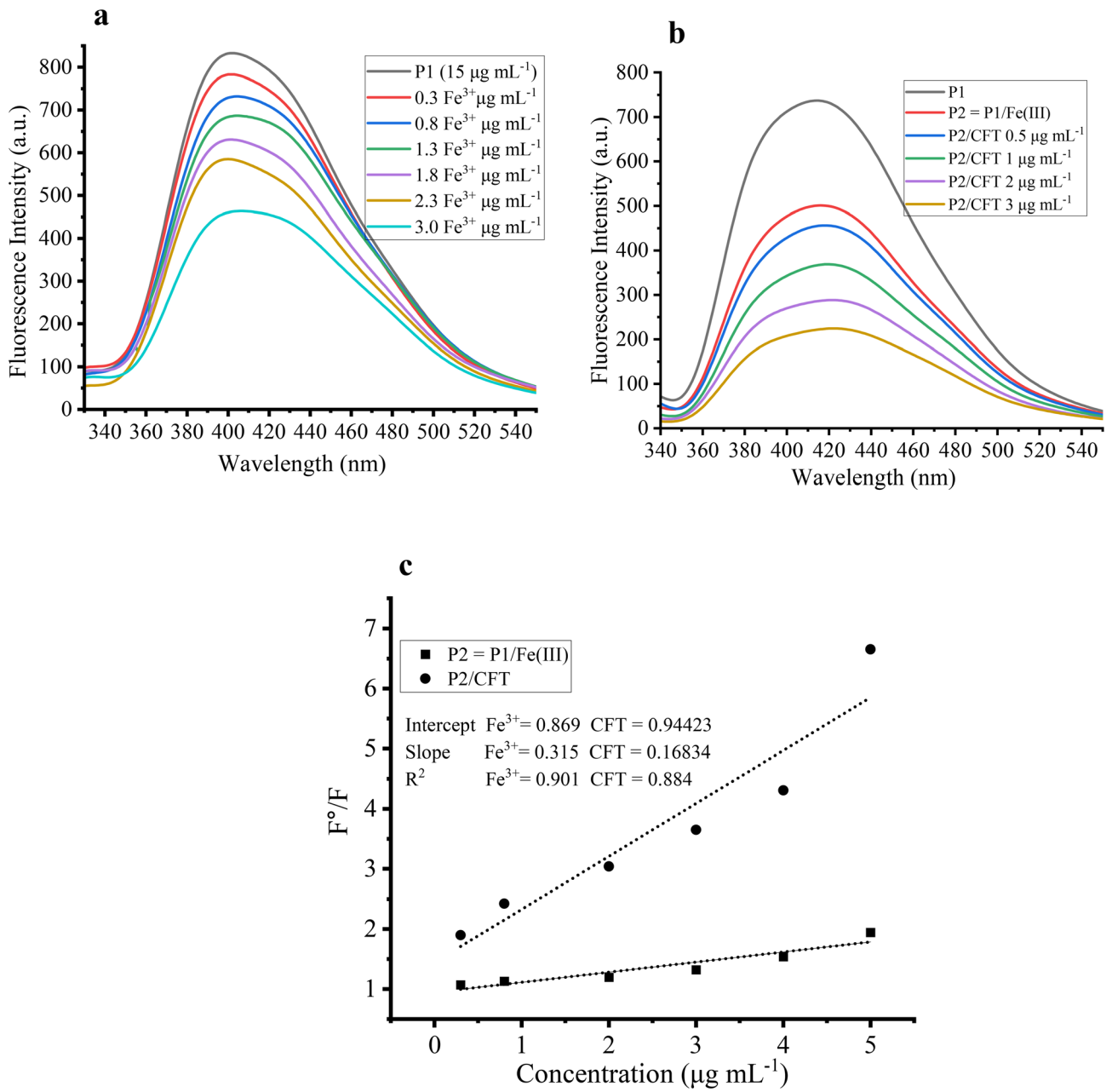

Fig. 5 (a) Effect of concentration of Fe^{3+} on FI of P1 in methanol–water mixture ($\lambda_{ex} = 320$ nm, $\lambda_{em} = 420$ nm). (b) Effect of CFT concentration on FI of P2 complex. (c) Calibration curve for the determination of Fe(III) and CFT.

functional group such as –OH, as a result, conjugation provides resonance stabilization, making the Schiff's bases less reactive towards hydrolysis. In the case of a complex, Schiff's base coordinates with metal ions by the imine group and donor atoms like oxygen, improving delocalization of electrons between the ligand and metal ion, leading to the formation of a stable complex. So, the P1 and its complex are stable due to the conjugation and chelation with Fe(III) as a function of time.

3.7. Interference effect

The interference effect of various metal ions, including Zn, Cd(II), Co(II), Ni(II), Pb(II), Fe(II), Hg(II), Mg(II), Na(I), Ca(II), Sn(II), Pd(II), Mn(II), Cr(III), Ag(I) and Cu(II), was investigated to determine the influence of other metal ions on the determination of Fe(III) ions. It was observed that fluorescence quenching is not substantially affected by the presence of interfering ions except Co(II) and Fe(II), which exhibited insignificant interaction with P1 (Fig. 4a).

3.8. Linearity study

The linear relationship of Fe(III) concentration in the range of 0.3–3.0 μg mL^{-1} and the fluorescence quenching of P1 was studied by a fluorescent titration experiment. As depicted in Fig. 5a, the fluorescent intensity (FI) of P1 (15 μg mL^{-1}) linearly decreases as the concentration of Fe(III) increases. The solvent

system used was a methanol–water mixture (2 : 3 v/v, total of 5.0 mL), as a medium for the interaction between P1 and Fe(III). Different analytical parameters, such as standard deviation (SD), and limit of detection (LOD), were determined based on replicate analysis at the lowest quantifiable concentration of Fe(III), which was 0.4 μg mL^{-1}. The limit of detection (LOD) value calculated for Fe(III) was 0.08 μg mL^{-1}, indicating the reliable development of the analytical method for the quantitative determination of Fe(III) using P1 as chemosensor. The results obtained demonstrate the applicability of the developed method for detecting Fe(III) in water samples.

3.9. Reversibility study

The reversibility of the interaction between the P1 and Fe(III) was investigated using the chelating agent ethylenediaminetetraacetic acid (EDTA). When EDTA was added to the mixture of the P2, the fluorescence intensity was found to restore, as shown in Fig. 6a. This indicated that the Fe(III) interacted reversibly with P1 and formed a complex with EDTA.

3.10. Job's plot analysis

The binding ratio between the chemosensor P1 and Fe(III) was determined using Job's plot analysis. An equimolar amount of

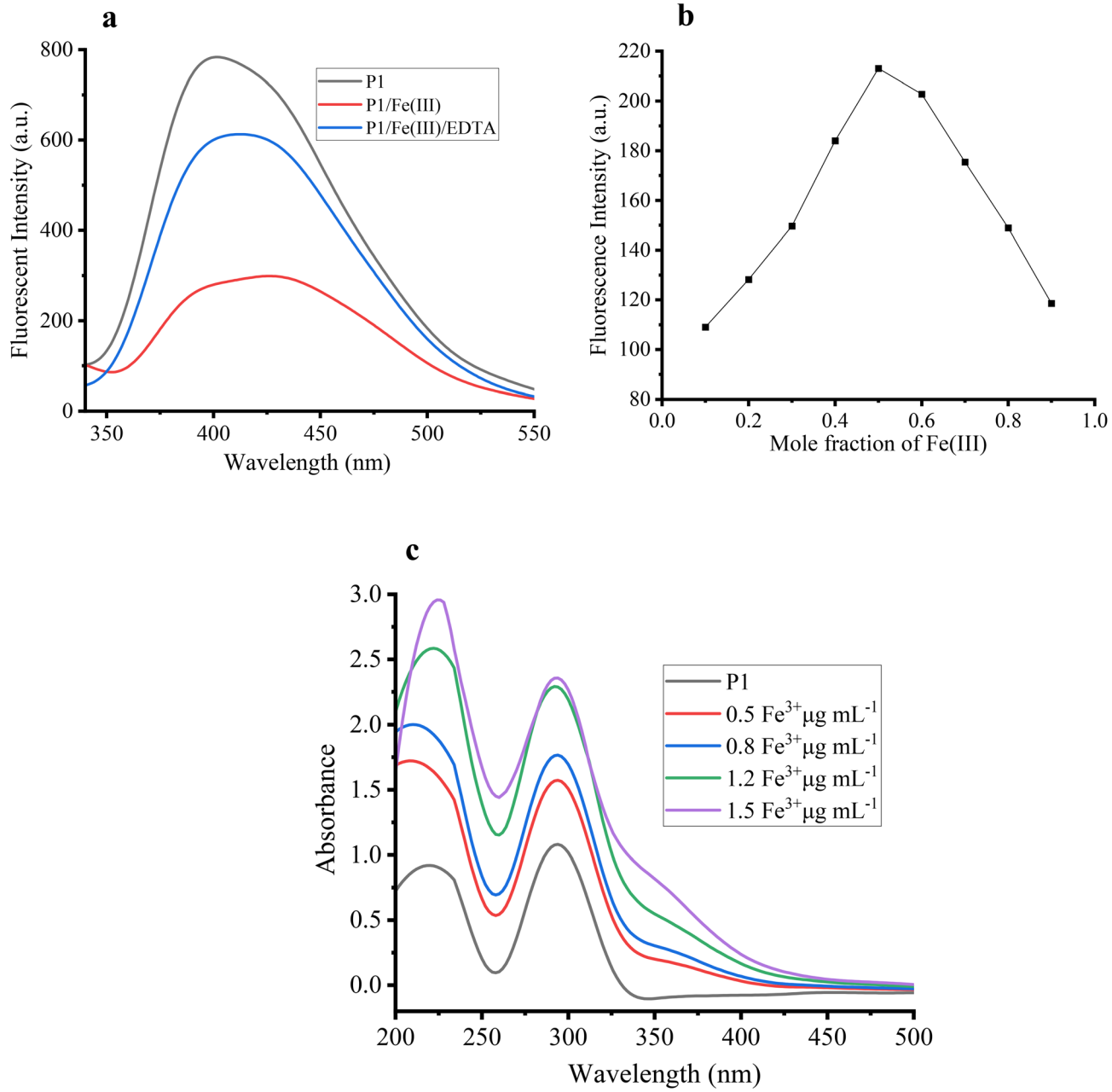

Fig. 6 (a) Reversibility determination of P2 in the presence of EDTA (b) Job's plot analysis between P1 and Fe(III) (c) UV-vis. Absorption spectra of P1 and different concentrations of Fe(III) with P1.

Table 1 Analytical figures of merit for the determination of Fe(III) and CFT

Parameters	Fe(III)	CFT
$\lambda_{ex\ (nm)}$	320	320
$\lambda_{em\ (nm)}$	420	420
Linearity range (μg mL^{-1})	0.3–3.0	0.5.0–5.0
Regression equation	$y = 0.3146x + 0.8697$	$y = 0.8583x + 0.6591$
Regression coefficient (R^2)	0.90	0.88
SD (μg mL^{-1})	0.008	0.03
LOD (μg mL^{-1})	0.08	0.12
LOQ (μg mL^{-1})	0.28	0.40

Table 2 Comparison of the proposed method with the literature methods for Fe(III)

Probe	Test media	LOD (μM)	Linear range	Ref.
SUMOF-7II	Water	16.6	16.6–167	46
Fe-ISE	Water	10	1.0×10^{-2}–1.0×10^{-4} mol L^{-1}	47
Imidazole derivative	DMSO	4.8	—	48
Schiff base	DMSO : Water 50 : 50	4.13	—	49
Schiff base	DMF : Water 9 : 1	2.86	—	50
Schiff base	DMF	2.17	—	51
Schiff-base	ACN	3.02	—	52
Schiff base	Methanol : Water 2 : 3	1.4	0.3–3.0 μg mL^{-1}	This work

P1 and Fe(III) (50 μM) was prepared, followed by mixing different volumes from 0.1–0.9 mL of P1 and 0.9–0.1 mL of Fe(III) to obtain a mole fraction of 1 : 9 to 9 : 1 in 5.0 mL volumetric flasks. The fluorescence intensity at 420 nm was plotted against the molar fraction of Fe(III). It was observed that the maximum fluorescence quenching occurs at a 0.5 molar fraction of Fe(III), as shown in Fig. 6b, indicating a metal-to-ligand ratio of 1 : 1.

3.11. UV-visible spectrophotometry

UV-visible spectroscopic property of chemosensor P1 and its interaction with Fe(III) was investigated. The free P1 showed two absorption peaks at 230 nm and 330 nm, respectively. As a result, π–π* and *n*–π* transition of electrons occurred. Upon the addition of Fe(III), a new band appeared at 360 nm and the persistent peaks of the P1 also increased, indicating the interaction between P1 and Fe(III) following ligand to metal charge transfer (LMCT) process. The absorption of P2 complex increased by increasing the Fe(III) concentration. The results are shown in Fig. 6c.

3.12. Proposed sensing mechanism for the detection of Fe(III)

The decrease in fluorescence intensity of the chemosensor P1 fluorophore upon the addition of Fe(III) can be attributed to the formation of a complex between P1 and Fe(III). The P1 exhibits conjugation characteristics with the non-bonding electrons on heteroatoms, making it fluorescent. The photophysical properties of the fluorescent chemosensor change on interaction with the electron acceptor or donor species. The paramagnetic behavior of transition metal ions, which could be involved in electron/energy transfer processes with organic fluorophores, results in a non-radioactive deactivation channel. Here, a P1 binding interaction with Fe(III) induced charge transfer (CT) from the donor ligand towards the acceptor Fe(III).[44] This ligand-to-metal charge transfer (LCMT) causes a decrease in π-conjugation, thus leading to the quenching of fluorescence. The reduction in fluorescence was such that the chemosensor displayed "turn-off" mode on interaction with Fe(III). On the contrary, P1 binding interaction with other metal ions was insignificant and did not substantially quench the fluorescence

Table 3 Comparison of the proposed method with the literature methods of CFT

Method	LOD (μg mL^{-1})	LOQ (μg mL^{-1})	Range (μg mL^{-1})	Ref.
Spectrophotometric	0.87504	2.92	2–24	53
Voltammetric	1.19	3.98	5–400	54
Spectrofluorimetric	0.2804	—	4–25	55
Capillary zone electrophoresis (CZE)	> 0.5	—	2–160	56
Spectrophotometric	0.750	2.740	1–70	57
LC-MS	0.301	0.993	1–40	58
Spectrofluorophotometric	0.12	0.4	0.5–4	This study

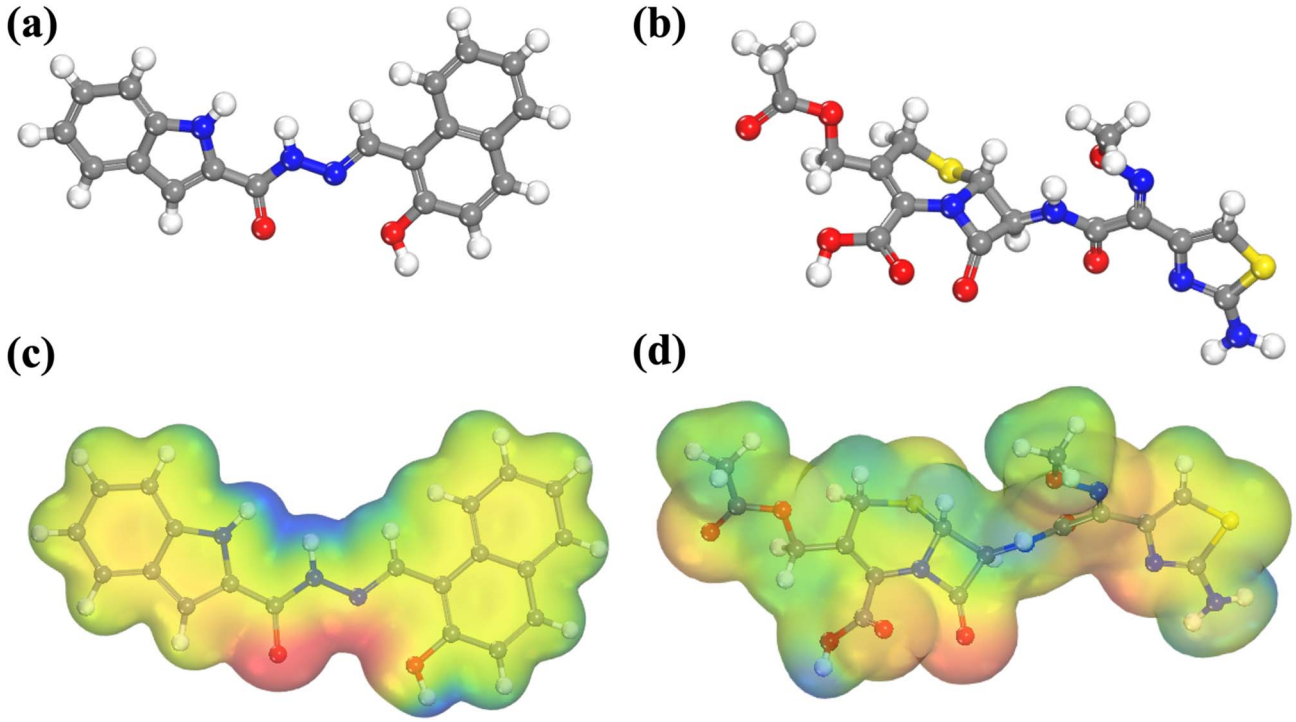

Fig. 7 Optimized geometry of (a) P1 and (b) CFT with their corresponding (c and d) MEP maps (isovalue = 0.03 a.u.).

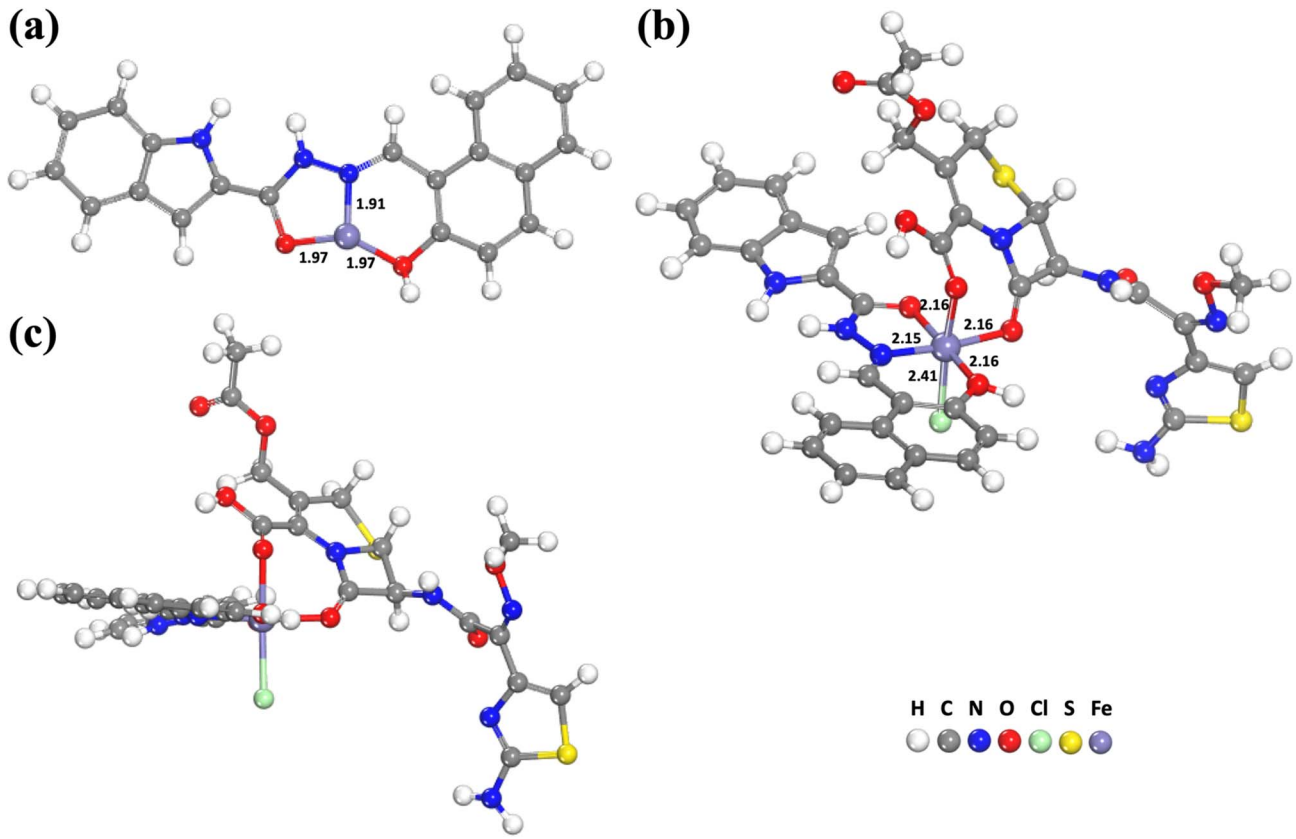

Fig. 8 (a) Optimized geometry of P1/Fe(III) and (b) Fe((P1-CFTCl)) complex (c) Top view and side view. All bond distances are in Å.

Table 4 Total electron density (ρ a.u.), laplacian of the electron density ($\nabla^2 \rho$ a.u.) and electron energy density ($H(r)$ a.u.) at various BCPs for the complex

BCP	ρ (r) (a.u.)	$\nabla^2 \rho(r)$ (a.u.)	$H(r)$ (a.u.)
BCP129, H(18)···H(78)	0.001	0.004	0.00024
BCP161, O(45)···Fe(41)	0.071	0.534	0.00469
BCP162, O(48)···Fe(41)	0.071	0.520	0.00406
BCP169, O(11)···Fe(41)	0.079	0.578	0.00205
BCP173, O(27)···Fe(41)	0.065	0.568	0.00895
BCP174, N(13)···Fe(41)	0.111	0.765	−0.01524
BCP175, Cl(42)···Fe(41)	0.045	0.190	−0.00566

intensity. The lack of interaction could be due to the different coordination geometry of P1, the ionic radius differences, or the low binding energy of these metal ions.

3.13. Fluorescence quenching of P2 by CFT

The P2 complex was used as a dual probe for the detection of the antibiotic cefotaxime sodium. As the CFT concentration increased in the range of 0.5–5 μg mL^{-1}, the fluorescent intensity was found to further decrease linearly, as shown in Fig. 5b. This persistent decrease in fluorescence demonstrated the ability of the P2 complex to selectively determine the CFT, making it a convenient method for pharmaceutical analysis. To evaluate the analytical parameters of the P2 complex for CFT detection, replicate analysis of 0.5 μg mL^{-1} of CFT was carried out for the calculation of SD, LOD, and LOQ values. The values were calculated for LOD and LOQ of 0.12 μg mL^{-1} and 0.4 μg mL^{-1}, respectively, using standard equations 3.3 S b^{-1} for LOD and 10 S b^{-1} for LOQ as shown in Table 1. These results indicate the suitability and accuracy of the P2 complex for sensing low concentrations of CFT, suggesting its applicability in pharmaceutical monitoring and quality control.

3.14. Effect of common excipients and metal ions

The selectivity of the proposed method was explored in the presence of meta ions and common excipients associated with the matrix of the subject antibiotics. The probe P2 was applied for the determination of CFT in the presence of common

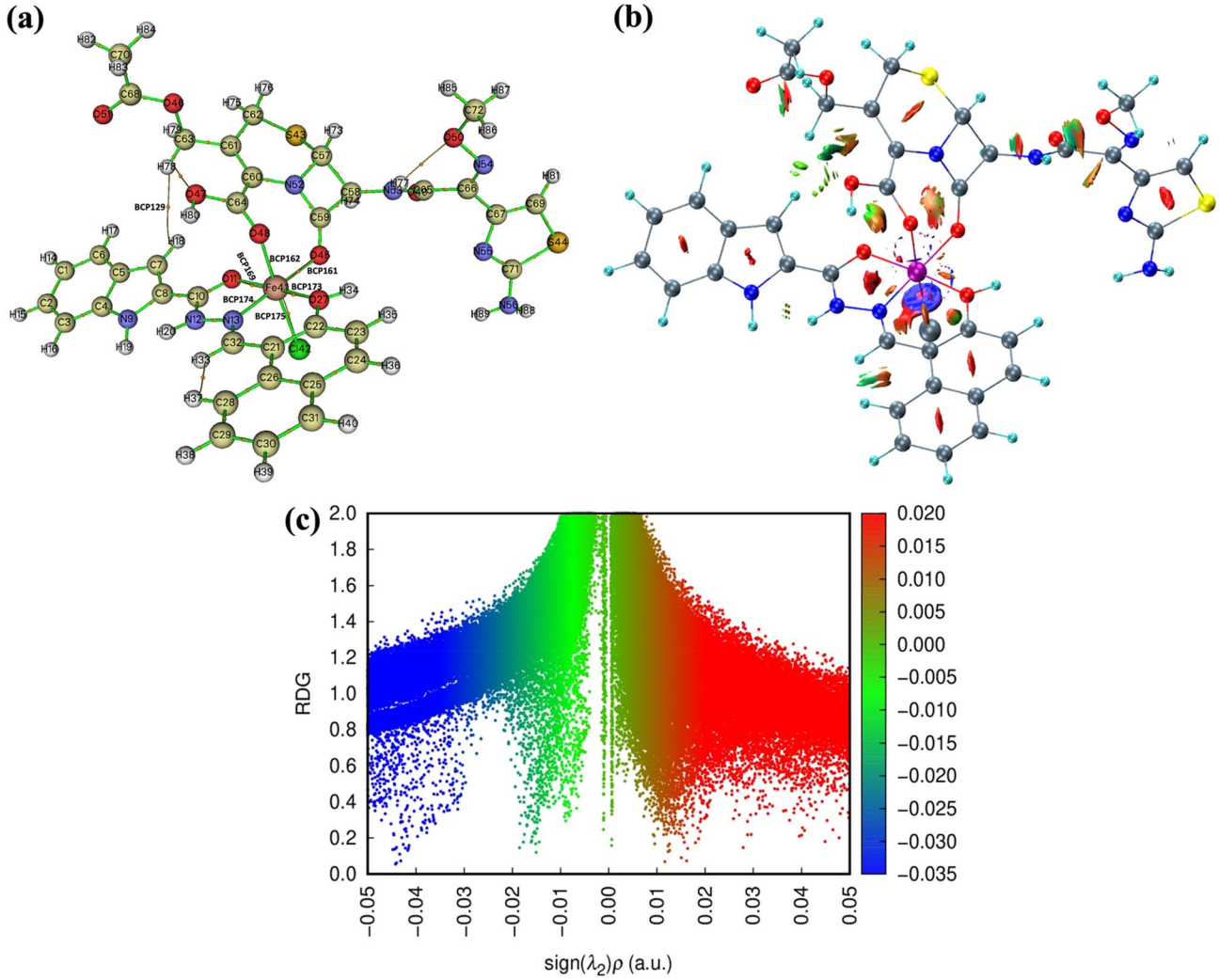

Fig. 9 (a) QTAIM molecular graph, (b) RDG isosurface, and (c) NCI scattered plot of Fe(P1-CFTCl) complex. BCPs show bond critical points.

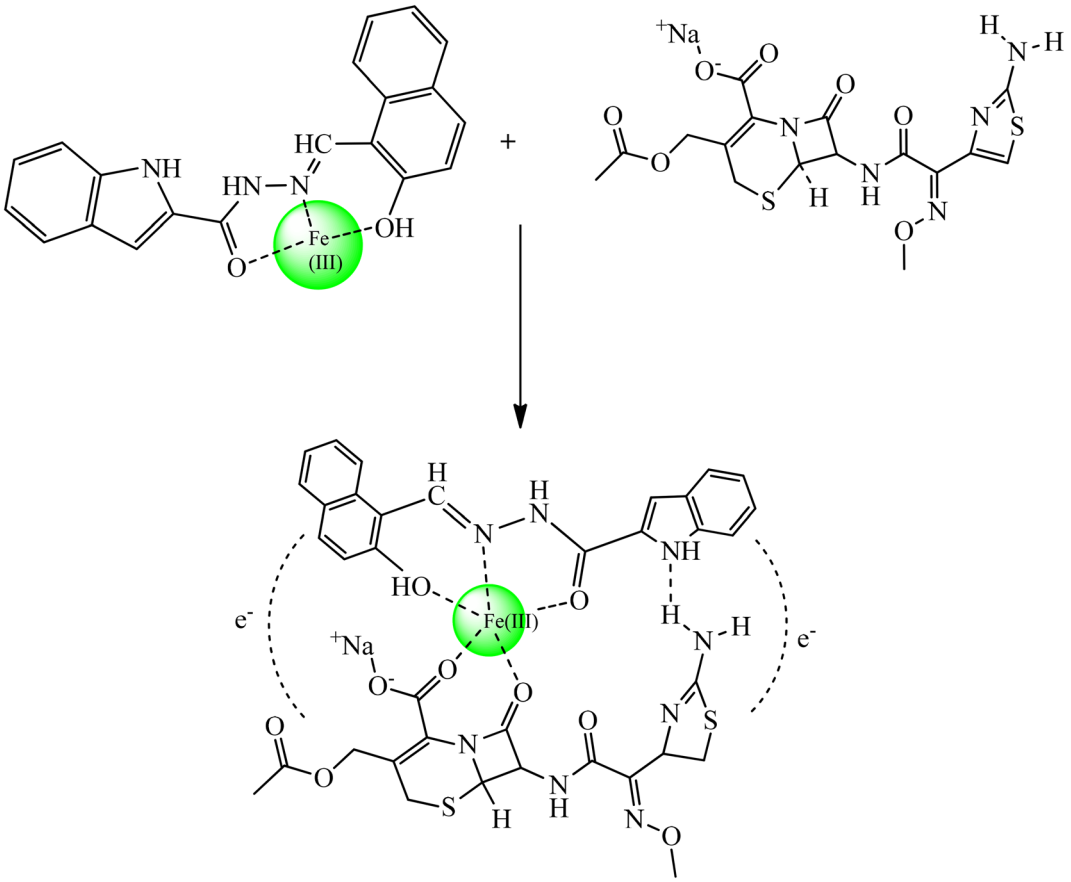

Scheme 2 Proposed sensing mechanism of CFT using P2.

excipients such as glucose (Glu), gum, citric acid (C acid), folic acid (F acid), and fructose (Fru) and metal ions including Na(I), Mg(II), Ca(II), Mn(II), Co(II), Ni(II), Fe(II), Cr(III), Fe(III), Ag(I), Sn(II), *etc.* It was observed that the fluorescence quenching ($F°/F$) is not affected even in the presence of common excipients and different metal ions excluding insignificant interaction of Co(II) and Fe(II), whereas Fe(III) showed slight interaction on CFT determination. The results are shown in Fig. 4b and c, indicating the selectivity of the complex P2 for CFT determination.

3.15. The proposed sensing mechanism for CFT using P2

The fluorometric determination of cefotaxime sodium (CFT) antibiotic was investigated using P2 as a sensing probe. The fluorescence quenching of the probe caused by CFT might be attributed to dynamic, static, or both, depending on the interaction involved between the fluorophore and the analyte (antibiotic). The quencher perturbed the electronic density of the chemosensor P1 due to Vander Waal's interaction following a static quenching approach. This type of interaction leads to a decrease in the fluorescence intensity of the fluorophore. Here, the P1 formed interaction with Fe(III) as well as non-covalent interactions with CFT, which affects the conjugation, resulting in the attenuation of the P1 fluorescence intensity. Another possible reason for fluorescence quenching with CFT is the inner filter effect, resulting from the absorption of radiation that causes the excitation of fluorophore P1.[45] Here, the proposed sensing scheme was designed according to the computational approach using DFT, NCI, and QTAIM analyses as mentioned later in the computational study.

3.16. Comparative study

Literature on different analytical methods for the determination of Fe(III) and cefotaxime sodium antibiotic was studied and the results are given in Table 2 and 3, respectively. Different statistical parameters in terms of percent recovery, LOD, and

Table 5 Application of the proposed method to the determination of Fe(III) in water samples

Sample	Amount added ($\mu g\ mL^{-1}$)	Amount found ($\mu g\ mL^{-1}$)	% recovery	Average % recovery ± SD
Tap water	0.5	0.504	101.0	99.4 ± 2.3
	0.5	0.49	97.7	
	1.0	0.99	98.6	97.9 ± 1.0
	1.0	0.97	97.1	
Pond water	0.5	0.53	106.1	103.8 ± 3.4
	0.5	0.51	101.4	
	1.0	0.95	95.4	98.2 ± 4.0
	1.0	1.01	101.0	

Table 6 Percent recovery of CFT from serum and commercial formulation

Sample	Amount added (μg mL^{-1})	Amount found (μg mL^{-1})	% recovery	Average % recovery ± SD
Serum	1.0	0.95	94.7	96.9 ± 1.9
		0.98	97.9	
	2.0	1.8	90.5	95.2 ± 6.6
		1.9	99.8	
Commercial formulation	1.0	0.96	95.9	96.6 ± 1.0
		0.97	97.4	
	2.0	1.8	91.3	92.4 ± 1.5
		1.8	93.5	

solvent system of the previously reported methods were compared with those of the proposed method. In this regard, the current study showed comparable results or even better in some parameters, like solvent system and LOD values. This highlights the validity and accuracy of the P1 and P2 dual probes, confirming their sensing applications in different analytical contexts.

3.17. Computational study

The optimized geometry of P1 and CFT, along with their molecular electrostatic potential (MEP) maps, are presented in Fig. 7. The red, yellow-green and blue regions in the MEP maps demonstrate electron-rich, moderate, and electron-deficient regions in P1 and CFT molecules.[59] Considering the MEP map (Fig. 7c), the interaction of the P1 molecule with the Fe(III) ion was evaluated through DFT calculation under the implicit solvent model (COSMO). The highly negative E_b value (−2.42 eV), calculated by equation (i), supports the thermodynamically feasible interaction of P1 with Fe(III) ion in aqueous medium. As evident from the optimized geometry of P2 complex (Fig. 8a), the capturing of Fe(III) ion by P1 is made possible by C=O···Fe, HO···Fe, and N···Fe interactions with 1.97, 1.97, and 1.91 Å bond lengths, respectively. Similarly, the optimized geometry of CFT shows that the two adjacent carbonyl groups (C=O) are likely the most effective sites for interaction with the P2 complex. Thus, interacting P2 with CFT and eventually a Cl^- ion gives rise to a stable octahedral type of complex as reflected by their respective E_b values of −2.14 eV and −4.60 eV, shown in Fig. 8b. The central Fe(III) ion has almost identical bond distances of 2.16 Å with various groups in the complex, in addition to a 2.41 Å length of the Fe–Cl bond.

The QTAIM and NCI analyses were performed to get an insight into the nature and strength of bonding between the P1, CFT, and Cl^- ligands with the Fe(III) ion in the complex. The QTAIM parameters are provided in Table 4. According to Bader's Quantum theory of Atoms in Molecules, if the ρ(a.u.) > 0.10, the $\nabla^2\rho$(a.u.) < 0, and H(a.u.) < 0 at a given BCP, the interaction would be a shared-shell (covalent) interaction. Alternatively, if the ρ(a.u.) is in the range of 0.02–0.06, the $\nabla^2\rho$(a.u.) > 0, and H(a.u.) < 0 at a particular BCP, the interaction would be designated as polar covalent bond. However, the interaction would be rendered closed-shell (electrostatic), characteristics of ionic, Vander Waal's interaction, or weak hydrogen bonding, when both the parameters (ρ and $\nabla^2\rho$) are positive.[60–62]

Considering the above criteria, the interactions of all the oxygen sites with the Fe^{3+} ion in the complex, represented by the BCPs (161, 162, 169, and 173) in the molecular graph (Fig. 9a), show a strong Fe–O interaction with a considerable degree of electrostatic character owing to the high electronegativity of oxygen. In addition, the BCP129 with very low ρ (0.001 a.u.) along the bond path $H(18)\cdots H(78)$ elucidates a weak van der Waals interaction between the CS and Cef ligands. Besides, the BCP174 and BCP175 in the molecular graph reflect a dative type (donor–acceptor) interaction with appreciable covalent characters, *i.e.*, coordinate covalent bonding between the N and Cl sites with the central Fe(III) ion. Conclusively, theoretical analyses suggested the formation of an octahedral type of complex (Fe(P1-CFTCl)) from the interaction of P1 and CFT with $FeCl_3$ in aqueous medium, stabilized through coordinate covalent bonding, electrostatic interaction and weak van der Waals' forces.

The presence of NCI prevailed in the complex is further verified by 3D spatially visualized isosurfaces using colored patches, called isosurfaces, differentiating attractive interaction, van der Waals, and steric repulsive interactions by blue, green, and red colors, respectively (shown in Fig. 9b).[63] Thus, the observed greenish patches between P1 and CFT further support the existence of van der Waals interaction between these ligands. Likewise, the scattered graph of the complex, displayed in Fig. 8c, is the plot of RDG S *vs.* (sign λ_2)ρ. Accordingly, the negative values (sign λ_2)ρ < 0 illustrate attractive interactions, whereas the positive values (sign λ_2)ρ > 0 signify repulsive interactions.[37,64] Hence, the green spikes (around −0.02 a.u.) and blue spikes in between −0.04 and −0.05 a.u. on the left side of the scattered graph (Fig. 9c) validate the presence of van der Waals and strong attractive forces in the complex. DFT results also revealed the same approach for the interaction of active sites of P1 with Fe(III) as shown in the proposed Scheme 2.

3.18. Applications

The dual probe chemosensor P1 was used to investigate Fe(III) in tap and pond water. Subsequently, P2 was further employed for the detection of CFT antibiotic in serum and commercial formulations. Tap and pond water were spiked with a known concentration of Fe(III) (0.5 and 1.0 μg mL^{-1}). Similarly, the serum samples were spiked with a known concentration of CFT

(1.0 and 2.0 μg mL^{-1}), and the CFT was also determined in the commercial formulation (market tablet), having amounts 1.0 and 2.0 μg mL^{-1}, respectively. It was noticed that the developed method showed good percent recoveries in the range of 92 to 97% for both the target analytes Fe(III) and CFT. All the results obtained are tabulated in Table 5 and 6 and suggest the applicability of the developed method for the determination of Fe(III) and CFT in the given samples.

4 Conclusion

In the current study, an indole-based chemosensor (P1) was investigated for the detection of Fe(III) based on fluorescence quenching of P1. The complex P2 was further employed as a dual probe for the determination of CFT based on a further decrease in FI. Excellent linearity was found for the detection of both the analytes *i.e.* Fe(III) and CFT, in a methanol–water system at pH 7. The optimized conditions were thoroughly explored including concentration, solvents, time and competent interferents. Under the optimum conditions, the P1 was investigated for the quantitative determination of Fe(III), and the P2 complex was further employed for the detection of CFT antibiotic in serum and commercial formulation. The analytical validation of the proposed method was carried out by calculating LOD and LOQ, which were found to be 0.08 and 0.28 μg mL^{-1} for Fe(III) and 0.12 and 0.4 μg mL^{-1} for CFT, respectively. Other parameters such as SD and RSD were also calculated with very low values and exhibited high precision along with good percent recoveries in the range of 97.9 ± 1.0% to 103.8 ± 3.4% for Fe(III) and 92.4 ± 1.5 to 96.9 ± 1.9% for CFT. Similarly, the highly negative E_b values of −2.42 and −4.60 eV for P2 and P1/FeCFTCl, respectively, predicted the energetically feasible formation of the complexes. Moreover, the calculated values of $\nabla^2\rho(r)$ and $H(r)$ values at the observed BCPs suggested the stabilization of the complex (P2CFTCl) through coordinate covalent bonds and electrostatic and van der Waals interactions. These results show the reliability and validity of the chemosensor. The developed method is dual, fast, simple, and interference-free, making it a suitable approach for determining Fe(III) and CFT in environmental and biological samples.

Conflicts of interest

There are no conflicts to declare.

Data availability

All data supporting the findings of this study, including spectral data, figures, statistical parameters, and characterization files, are provided in the article and supplementary information (SI). Supplementary information: figures showing synthesis schemes, FTIR and ^{1}H NMR spectra, data of replicate measurements for calculation of statistical parameters, raw data of application of the proposed methods, raw data of interference studies and raw data of spectrofluorimetric response of the proposed sensors as a function of the concentration of the subject analytes. All the figures and tables have been cited in the text of the manuscript. See DOI: https://doi.org/10.1039/d5ra09532h.

Acknowledgements

This research was supported by the University of Malakand and Higher Education Commission (HEC) of Pakistan project no. 20-14499/NRPU/R&D/HEC/2021.

References

1 A. Singh, R. Pal, C. Gangwar, A. Gupta and A. Tripathi, Release of heavy metals from industrial waste and e-waste burning and its effect on human health and environment, *Int. J. Emerg. Res. Manag. Technol.*, 2015, **4**(12), 51.
2 F. Akbal and S. Camcı, Copper, chromium and nickel removal from metal plating wastewater by electrocoagulation, *Desalination*, 2011, **269**(1–3), 214–222.
3 Y. Zhou, J. F. Zhang and J. Yoon, Fluorescence and colorimetric chemosensors for fluoride-ion detection, *Chem. Rev.*, 2014, **114**(10), 5511–5571.
4 V. N. Mehta, S. K. Kailasa and H. F. Wu, Sensitive and selective colorimetric sensing of Fe 3+ ion by using p-amino salicylic acid dithiocarbamate functionalized gold nanoparticles, *New J. Chem.*, 2014, **38**(4), 1503–1511.
5 S. Rattanopas, P. Piyanuch, K. Wisansin, A. Charoenpanich, J. Sirirak, W. Phutdhawong and N. Wanichacheva, Indole-based fluorescent sensors for selective sensing of Fe2+ and Fe3+ in aqueous buffer systems and their applications in living cells, *J. Photochem. Photobiol., A*, 2019, **377**, 138–148.
6 P. Aisen, M. Wessling-Resnick and E. A. Leibold, Iron metabolism, *Curr. Opin. Chem. Biol.*, 1999, **3**(2), 200–206.
7 O. K. Fix and K. V. Kowdley, Hereditary hemochromatosis, *Minerva Med.*, 2008, **99**(6), 605–617.
8 M. D. Beaton and P. C. Adams, The myths and realities of hemochromatosis, *Can. J. Gastroenterol. Hepatol.*, 2007, **21**(2), 101–104.
9 J. D. Haas and I. V. T. Brownlie, Iron deficiency and reduced work capacity: a critical review of the research to determine a causal relationship, *J. Nutr.*, 2001, **131**(2), 676S–690S.
10 N. Khatri, S. Tyagi and D. Rawtani, Recent strategies for the removal of iron from water: A review, *J. Water Proc. Eng.*, 2017, **19**, 291–304.
11 J. L. Martinez and J. Olivares, Environmental pollution by antibiotic resistance genes, *Antimicrob. Resist. Environ.*, 2012, **34**, 151–171.
12 F. Aarestrup, Get pigs off antibiotics, *Nature*, 2012, **486**(7404), 465–466.
13 *Pharmaceutical Innovation: Revolutionizing Human Health*, ed. R. Landau, B. Achilladelis and A. Scriabine. Chemical Heritage Foundation, 1999.
14 D. Chen, H. Wang, Z. Zhang, L. Ci and X. Zhang, Chemiluminescence determination of cefotaxime sodium with flow-injection analysis of cerium (IV)–rhodamine 6G system and its application to the binding study of cefotaxime sodium to protein with on-line microdialysis sampling, *Spectrochim. Acta, Part A*, 2011, **78**(1), 553–557.

15 M. Bilal, S. Mehmood, T. Rasheed and H. M. Iqbal, Antibiotics traces in the aquatic environment: persistence and adverse environmental impact, *Curr. Opin. Environ. Sci. Health*, 2020, **13**, 68–74.
16 J. L. Martinez, Environmental pollution by antibiotics and by antibiotic resistance determinants, *Environ. Pollut.*, 2009, **157**(11), 2893–2902.
17 X. Mu, Z. Huang, O. E. Ohore, J. Yang, K. Peng, S. Li and X. Li, Impact of antibiotics on microbial community in aquatic environment and biodegradation mechanism: a review and bibliometric analysis, *Environ. Sci. Pollut. Res.*, 2023, **30**(25), 66431–66444.
18 U. Araujo-Barbosa, E. Peña-Vazquez, M. C. Barciela-Alonso, S. L. Ferreira, A. M. Dos Santos and P. Bermejo-Barrera, Simultaneous determination and speciation analysis of arsenic and chromium in iron supplements used for iron-deficiency anemia treatment by HPLC-ICP-MS, *Talanta*, 2017, **170**, 523–529.
19 M. R. Pourjavid, M. Arabieh, S. R. Yousefi and A. A. Sehat, Interference free and fast determination of manganese (II), iron (III) and copper (II) ions in different real samples by flame atomic absorption spectroscopy after column graphene oxide-based solid phase extraction, *Microchem. J.*, 2016, **129**, 259–267.
20 J. Proch and P. Niedzielski, Iron species determination by high performance liquid chromatography with plasma based optical emission detectors: HPLC–MIP OES and HPLC–ICP OES, *Talanta*, 2021, **231**, 122403.
21 A. S. Andreani, E. S. Kunarti, T. Hashimoto, T. Hayashita and S. J. Santosa, Fast and selective colorimetric detection of Fe3+ based on gold nanoparticles capped with ortho-hydroxybenzoic acid, *J. Environ. Chem. Eng.*, 2021, **9**(5), 105962.
22 N. Esfandiari and M. Aliofkhazraei, Advances in the determination of trace amounts of iron cations through electrochemical methods: A comprehensive review of principles and their limits of detection, *Talanta*, 2024, **277**, 126365.
23 L. H. Jia, Y. Chen, Q. Mao, D. Zhang, J. Yuan, X. Li, S. Wu and D. Zhang, Simultaneous in-situ determination of major, trace elements and Fe 3+/$\sum$ Fe in spinel using EPMA, *At. Spectrosc.*, 2022, **1**, 43.
24 A. F. e Silva, W. V. de Castro and F. P. de Andrade, Development of spectrophotometric method for iron determination in fortified wheat and maize flours, *Food Chem.*, 2018, **242**, 205–210.
25 I. T. Humeidy, Spectrophotometric determination of cefotaxime sodium in pharmaceutical formulations, *Mater. Today: Proc.*, 2021, **47**, 6043–6049.
26 L. V. de Faria, T. P. Lisboa, N. da Silva Campos, G. F. Alves, M. A. Matos, R. C. Matos and R. A. Munoz, Electrochemical methods for the determination of antibiotic residues in milk: A critical review, *Anal. Chim. Acta*, 2021, **1173**, 338569.
27 E. T. Anwer, O. Porwal and R. Dudhe, Development and validation of RP-HPLC method for estimation of Cefotaxime sodium in bulk and formulation, *Res. J. Pharm. Technol.*, 2022, **15**(7), 3114–3118.
28 G. M. Khairy, A. S. Amin, S. M. Moalla, A. Medhat and N. Hassan, Fluorescence determination of Fe (III) in drinking water using a new fluorescence chemosensor, *RSC Adv.*, 2022, **12**(42), 27679–27686.
29 Q. U. Sandhu, M. Pervaiz, A. Majid, U. Younas, Z. Saeed, A. Ashraf, R. R. Khan, S. Ullah, F. Ali and S. Jelani, Schiff base metal complexes as anti-inflammatory agents, *J. Coord. Chem.*, 2023, **76**(9–10), 1094–1118.
30 G. Singh, P. Kalra, A. Arora, G. Sharma, A. Singh and V. Verma, Design and synthesis of indole triazole pendant siloxy framework as a chemo sensor for sensing of Cu2+ and Ni2+: A comparison between traditional and microwave method, *Inorg. Chim. Acta*, 2018, **473**, 186–193.
31 D. Choe, H. So, S. Park, H. Lee, J. B. Chae, J. Kim, K. T. Kim and C. Kim, An indole-based fluorescent chemosensor for detecting Zn2+ in aqueous media and zebrafish, *Sensors*, 2021, **21**(16), 5591.
32 M. Demurtas, A. Baldisserotto, I. Lampronti, D. Moi, G. Balboni, S. Pacifico, S. Vertuani, S. Manfredini and V. Onnis, Indole derivatives as multifunctional drugs: Synthesis and evaluation of antioxidant, photoprotective and antiproliferative activity of indole hydrazones, *Bioorg. Chem.*, 2019, **85**, 568–576.
33 B. Delley, An all-electron numerical method for solving the local density functional for polyatomic molecules, *J. Chem. Phys.*, 1990, **92**(1), 508–517.
34 J. P. Perdew, K. Burke and M. Ernzerhof, Generalized gradient approximation made simple, *Phys. Rev. Lett.*, 1996, **77**(18), 3865.
35 S. Grimme, Accurate description of van der Waals complexes by density functional theory including empirical corrections, *J. Comput. Chem.*, 2004, **25**(12), 1463–1473.
36 A. Klamt, The COSMO and COSMO-RS solvation models, *Wiley Interdiscip. Rev.: Comput. Mol. Sci.*, 2011, **1**(5), 699–709.
37 R. F. Bader, A quantum theory of molecular structure and its applications, *Chem. Rev.*, 1991, **91**(5), 893–928.
38 R. Laplaza, F. Peccati, A. Boto R, C. Quan, A. Carbone, J. P. Piquemal, Y. Maday and J. Contreras-García, NCIPLOT and the analysis of noncovalent interactions using the reduced density gradient, *Wiley Interdiscip. Rev.: Comput. Mol. Sci.*, 2021, **11**(2), e1497.
39 T. Lu and F. Chen, Multiwfn: A multifunctional wavefunction analyzer, *J. Comput. Chem.*, 2012, **33**(5), 580–592.
40 W. Humphrey, A. Dalke and K. Schulten, VMD: visual molecular dynamics, *J. Mol. Graph.*, 1996, **14**(1), 33–38.
41 D. Wencel, T. Abel and C. McDonagh, Optical chemical pH sensors, *Anal. Chem.*, 2014, **86**(1), 15–29.
42 N. Mergu and V. K. Gupta, A novel colorimetric detection probe for copper (II) ions based on a Schiff base, *Sens. Actuators, B*, 2015, **210**, 408–417.
43 W. Pan, X. Yang, Y. Wang, L. Wu, N. Liang and L. Zhao, AIE-ESIPT based colorimetric and "OFF-ON-OFF" fluorescence Schiff base sensor for visual and fluorescent determination

of Cu2+ in an aqueous media, *J. Photochem. Photobiol., A*, 2021, **420**, 113506.

44 J. H. Chang, Y. M. Choe and Y. G. Sin, A significant fluorescence quenching of anthrylaminobenzocrown ethers by paramagnetic metal cations, *Bull. Korean Chem. Soc.*, 2001, **22**(5), 527–530.

45 F. Ali, M. Muhammad, B. Ara and A. A. Shah, Synthesis of fructose bound Fe (iii) integrated carbon dots as a robust turn-off detection sensor for chlortoluron, *RSC Adv.*, 2023, **13**(25), 17028–17037.

46 H. N. Abdelhamid, A. Bermejo-Gómez, B. Martín-Matute and X. Zou, A water-stable lanthanide metal-organic framework for fluorimetric detection of ferric ions and tryptophan, *Microchim. Acta*, 2017, **184**(9), 3363–3371.

47 M. Zareh, W. Zordek and A. Abd-Alhady, Iron-selective electrode based on phosphorylated calix-6-arene derivative, *J. Sens. Technol.*, 2014, **4**, 186–194.

48 G. Y. Gao, W. J. Qu, B. B. Shi, P. Zhang, Q. Lin, H. Yao, W. L. Yang, Y. M. Zhang and T. B. Wei, A highly selective fluorescent chemosensor for iron ion based on 1H-imidazo [4, 5-b] phenazine derivative, *Spectrochim. Acta, Part A*, 2014, **121**, 514–519.

49 C. Wang, J. Fu, K. Yao, K. Xue, K. Xu and X. Pang, Acridine-based fluorescence chemosensors for selective sensing of Fe3+ and Ni2+ ions, *Spectrochim. Acta, Part A*, 2018, **199**, 403–411.

50 S. A. Alahmady, S. Nazreen, A. Q. Alorabi and A. A. Elhenawy, Selective optical sensing of iron (III) ions in an aqueous medium by benzochromone-based Schiff base and its application on test strips, *Environ. Technol.*, 2024, **45**(8), 1542–1556.

51 X. Zhu, Y. Duan, P. Li, H. Fan, T. Han and X. Huang, A highly selective and instantaneously responsive Schiff base fluorescent sensor for the "turn-off" detection of iron (III), iron (II), and copper (II) ions, *Anal. Methods*, 2019, **11**(5), 642–647.

52 L. Yang, W. Zhu, M. Fang, Q. Zhang and C. Li, A new carbazole-based Schiff-base as fluorescent chemosensor for selective detection of Fe3+ and Cu2+, *Spectrochim. Acta, Part A*, 2013, **109**, 186–192.

53 I. T. Humeidy, Spectrophotometric determination of cefotaxime sodium in pharmaceutical formulations, *Mater. Today: Proc.*, 2021, **47**, 6043–6049.

54 K. Rudnicki, K. Sobczak, M. Kaliszczak, K. Sipa, E. Powałka, S. Skrzypek, *et al.*, Voltammetric study of cefotaxime at the macroscopic and miniaturized interface between two immiscible electrolyte solutions, *Microchim. Acta*, 2021, **188**(12), 413.

55 M. A. Omar, O. H. Abdelmageed and T. Z. Attia, Kinetic spectrofluorimetric determination of certain cephalosporins in human plasma, *Talanta*, 2009, **77**(4), 1394–1404.

56 R. Wang, Z. P. Jia, J. J. Fan, M. Jun, X. Hua, Q. Zhang, *et al.*, Separation and determination of cefotaxime enantiomers in injections by capillary zone electrophoresis, *Int. J. Pharma Sci.*, 2009, **64**(3), 156–160.

57 S. M. Abbas and M. N. Mohammed, Spectrophotometric Determination of Cefotaxime via Diazotization Reaction in Pure and Pharmaceutical Samples, *Ibn al-Haitham j. pure appl. sci.*, 2017, **30**(2), 151–160.

58 C. L. Saranya, J. C. Thejaswini, B. M. Gurupadayya and B. Y. Sruthi, Simultaneous determination of cefotaxime sodium and paracetamol by LC-MS, *IOSR J. Pharm.*, 2014, **4**, 12–18.

59 A. M. Bayoumy, M. Ibrahim and A. Omar, Mapping molecular electrostatic potential (MESP) for fulleropyrrolidine and its derivatives, *Opt. Quant. Electron.*, 2020, **52**(7), 346.

60 P. S. Kumar, V. Raghavendra and V. Subramanian, Bader's theory of atoms in molecules (AIM) and its applications to chemical bonding, *J. Chem. Sci.*, 2016, **128**(10), 1527–1536.

61 I. Rozas, I. Alkorta and J. Elguero, Behavior of ylides containing N, O, and C atoms as hydrogen bond acceptors, *J. Am. Chem. Soc.*, 2000, **122**(45), 11154–11161.

62 I. Alkorta, I. Rozas and J. Elguero, Theoretical study of the Si–H group as potential hydrogen bond donor, *Int. J. Quantum Chem.*, 2002, **86**(1), 122–129.

63 N. S. Venkataramanan, A. Suvitha, R. Sahara and Y. Kawazoe, A computational study on the complexation of bisbenzimidazolyl derivatives with cucurbituril and cyclohexylcucurbituril, *J. Inclusion Phenom. Macrocyclic Chem.*, 2021, **100**(3), 217–231.

64 N. S. Venkataramanan, A. Suvitha and Y. Kawazoe, Unravelling the nature of binding of cubane and substituted cubanes within cucurbiturils: A DFT and NCI study, *J. Mol. Liq.*, 2018, **260**, 18–29.